Electrochemical stability of lithium salicylato-borates as electrolyte additives in Li-ion batteries

Serife Kaymaksiz [a], Florian Wilhelm [a], Mario Wachtler [a,*], Margret Wohlfahrt-Mehrens [a], Christoph Hartnig [b], Irina Tschernych [b], Ulrich Wietelmann [b]

[a] ZSW, Zentrum für Sonnenenergie- und Wasserstoff-Forschung Baden-Württemberg, Helmholtzstr. 8, 89081 Ulm, Germany
[b] Rockwood Lithium GmbH, Trakehner Str. 3, 60487 Frankfurt am Main, Germany

HIGHLIGHTS

► Reduction and oxidation stabilities of bis(salicylato)borates are reported.
► A combined experimental and theoretical approach has been used.
► Lithium bis(5-fluorosalicylato)borate is reported for the first time.
► Salicylato ligands show higher reduction and lower oxidation stability than oxalato ligands.
► Variations in stability can be explained by substituent-induced electronic effects.

ARTICLE INFO

ABSTRACT

A systematic study has been performed for several chelato-borate complexes by combining electrochemical characterization and ab-initio calculations to reveal whether they are appropriate to be used as electrolyte components in Li-ion batteries. The chelato-borates used in this study are lithium bis(oxalato)borate (LiBOB), lithium salicylatooxalatoborate (LiSOB), lithium bis(salicylato)borate (LiBSB), lithium bis(3-methylsalicylato)borate, lithium bis(5-fluorosalicylato)borate, lithium bis(5-chlorosalicylato) borate, lithium bis(5-bromosalicylato)borate, and lithium bis(3,5-dichlorosalicylato)borate. A graphite electrode is chosen to study the cathodic stability, while $LiMn_2O_4$ is selected to estimate the anodic stability limits of these chelato-borates. Additionally, the oxidation potentials of these compounds are predicted by employing density functional theory (DFT) calculations. The CV studies of graphite electrodes in these electrolyte mixtures indicate that irreversible reduction of the oxalato and salicylato groups occurs at 1.6–1.8 and 0.9–1.3 V vs. Li/Li$^+$, respectively. Besides, irreversible oxidation of the bis(salicylato)borate anions between 4.3 and 4.8 V vs. Li/Li$^+$ is observed in the CV curves of $LiMn_2O_4$ electrodes, depending on the respective ligands around the central boron atom. The theoretical calculations are generally in line with the experimental observations. Furthermore, they help to explain the differences between the oxidation potentials of the anions, which are caused by the different groups that donate the electron and the respective substitution pattern.

1. Introduction

During the last decades lithium-ion batteries (LIBs) have penetrated daily life by being used in household electronics and portable electronic devices [1]. The superiority of LIBs over the alternatives is due to their lightness and compactness reaching a specific energy between 100 Wh kg^{-1} and 150 Wh kg^{-1} at potentials up to 4.2 V [2].

Beyond being the preeminent energy storage and power sources of the current technology, LIBs are nowadays designed to fulfill the high power and energy needs in areas such as automotive [3] and space applications [4]. In view of the extensive use of LIBs cost and safety have become major issues. Safety is related both to the electrode materials, the electrolyte, and their interactions. Today's state-of-the-art electrolytes use highly flammable solvents and conductive lithium salts which are corrosive. However, it is possible to improve the safety characteristics of these electrolyte systems by using functional additives, which is the easiest and most adequate way of obtaining safer electrolytes [5]. By introducing a new

component to the state-of-the-art electrolytes, enhanced cycling performance and desired safety features can be achieved. An additive can, for instance, play an efficient role in decreasing flammability, increasing overcharge tolerance, improving ion conduction, modifying the solid electrolyte interphase (SEI), and preventing Al corrosion [5].

One interesting class of substances, which has been proposed both as electrolyte salt and electrolyte additive, are lithium chelato-borate salts. The most well-known chelato-borate in the LIB community is lithium bis(oxalato)borate (LiBOB). The electrochemical properties of LiBOB (Fig. 1) and its behavior as an electrolyte salt or as an electrolyte additive for LIBs have been studied previously in detail (e.g. Refs. [6–11]). Thermal stability up to 300 °C, stabilization of the Al current collector up to 5 V vs. Li/Li$^+$, and stable SEI formation at the graphite surface even in propylene carbonate (PC) containing electrolytes have been mentioned [12–15]. Additionally, LiBOB is a non-toxic and low-cost alternative to LiPF$_6$ and has provided high anodic and cathodic stability and increased safety with several electrode materials [6,16,17]. But LiBOB has also some limitations such as lower conductivity [18] and higher interfacial impedance for carbon-based anodes as compared to LiPF$_6$ [19,20].

Apart from LiBOB, boron-based chelate complex anions with aromatic or aliphatic diols, or carboxylic acids, e.g. lithium bis[1,2-benzenediolato(2-)-O,O']borate, were introduced as a new class of lithium salts by Barthel et al. [21–26]. Their studies indicate that these large and bulky organoborate anions provide better charge delocalization and higher oxidation stability due to the covalent bonds in their structures. Additionally, the effect of an electron-withdrawing substituent such as fluorine on the oxidation stability of those anions was investigated, and a raise by 0.1 V per fluorine and chelate ligand was observed in the electrochemical stability window of benzenediolato borate [24].

Among the organo-borates, especially salicylato-based chelato-borates have attracted the interest of researchers. Aurbach et al. [27] studied the anodic and cathodic stabilities of lithium bis(salicylato) borate (LiBSB) as an electrolyte additive in a graphite/LiMn$_2$O$_4$ cell. Their results exhibited the contribution of this additive to the SEI formation on the surface of the graphite electrode by irreversible reduction at around 830 mV vs. Li/Li$^+$. Besides, this additive acted electrochemically on the cathode surface by forming a passivation film and thus suppressing further surface reactions. Sasaki et al. [28–31] studied lithium bis[3-methylsalicylato(2-)]borate (LiBMSB), lithium bis[3,5-dichlorosalicylato(2-)]borate (LiBCl$_2$SB), lithium bis[3,5,6-trichlorosalicylato(2-)]borate (LiBCl$_3$SB), lithium bis[5-bromosalicylato(2-)]borate (LiBBrSB), and lithium bis [5-chlorosalicylato(2-)]borate (LiBClSB). These investigations have consistently demonstrated the substituent effect on the thermal and electrochemical properties. The oxidation stabilities of these compounds on glassy carbon (GC) electrodes were reported to decrease in the order LiBCl$_3$SB ∼ LiBCl$_2$SB > LiBClSB > LiBBrSB > LiBSB > LiBMSB [28]. The reduction stability (on GC electrodes) decreased in the opposite order, except for LiBClSB. Furthermore the galvanostatic cycling behavior of these substances used as electrolyte additives at a concentration of 0.01 mol L^{-1} was studied in Li/V$_2$O$_5$ primary and Li/ CoO$_2$ and graphite/LiCoO$_2$ secondary cells. For Li/V$_2$O$_5$ cells the discharge capacity was increased, for Li/LiCoO$_2$ cells the cycling stability was increased, and for graphite/LiCoO$_2$ cells the results were ambiguous [28].

The aim of the present work is to broaden the current knowledge of the use of Li chelato-borates as electrolyte components for LIBs. In this context, several chelato-borate complexes with unsubstituted and substituted salicylato ligands, as shown in Fig. 1, have been synthesized and investigated: LiBOB, lithium salicylatooxalatoborate (LiSOB), lithium bis(salicylato)borate (LiBSB),
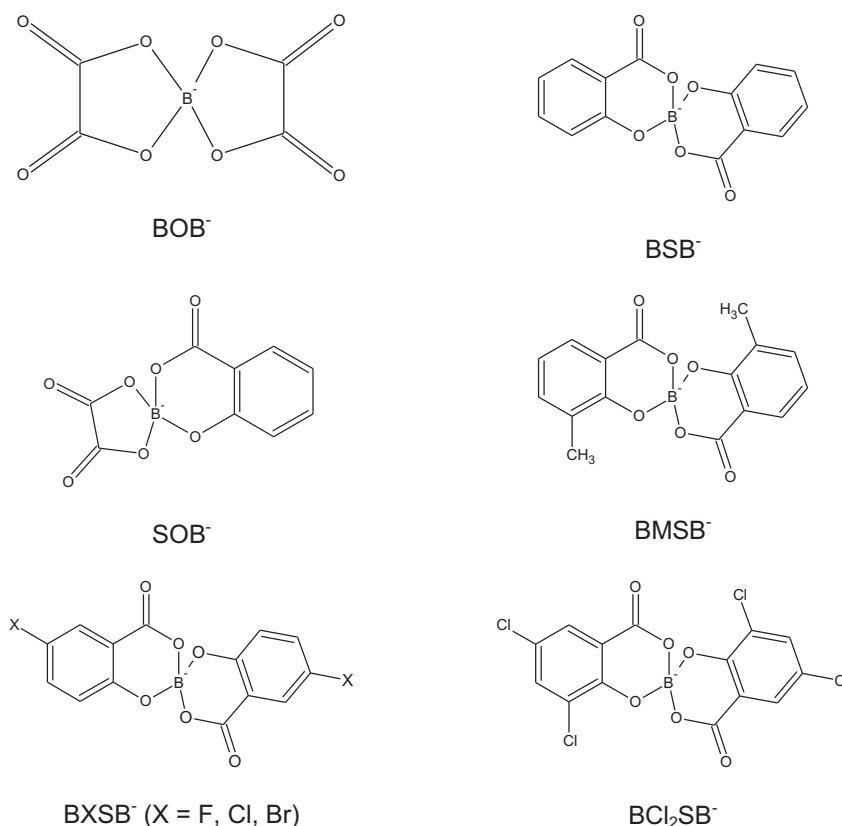

Fig. 1. Structural formulas of lithium chelato-borate anions.

lithium bis(3-methylsalicylato)borate (LiBMSB), lithium bis(5-fluorosalicylato)borate (LiBFSB), lithium bis(5-chlorosalicylato)borate (LiBClSB), lithium bis(5-bromosalicylato)borate (LiBBrSB), and lithium bis(3,5-dichlorosalicylato)borate (LiBCl$_2$SB). To the best of our knowledge, LiBFSB has been synthesized and studied for its electrochemical behavior for the first time. For LiSOB only the synthesis [32] and the reduction stability on GC [8,33] have been reported, so far, and data on the behavior with real electrode materials are lacking.

Generally, studies with "inert" electrodes such as Pt or GC, which do not insert Li$^+$, give a good first picture of redox stabilities. However, the confirmation of oxidation or reduction stability within a certain potential range at these electrodes does not automatically imply that the substance is also stable in contact with real electrode materials. Catalytic effects of cathode materials, the presence of reactive surface groups, and generally the presence of other faradaic processes in combination with significantly larger surface areas of real electrodes can induce reactions at potentials, where a substance would be stable in contact with Pt or GC [34]. In the case of graphite instability is even beneficial as long as the reduction products are able to form a SEI which prevents solvent cointercalation and subsequent graphite exfoliation. Therefore, the cathodic and anodic stability limits as well as the reversibility of the charging processes of the salicylato-borates under investigation were determined at real electrodes, namely graphite and LiMn$_2$O$_4$ electrodes, respectively, using cyclic voltammetry (CV). The experimentally observed oxidation stabilities were furthermore compared to the values obtained from theoretical calculations.

During the last decades, computational chemistry methods have become powerful tools to investigate molecular properties even if they are hardly accessible in experiment and to predict characteristics and behavior of molecules without the need of actually synthesizing them. Concerning possible additives for LIBs, especially density functional theory (DFT) has proved to be a very valuable tool to predict the reduction [35] and oxidation [36–39] potentials of molecules. Most of the studies published in this field deal with neutral aromatic molecules, but also some anionic compounds have been considered [40]. In view of the complexity of the oxidation behavior of the borate salts on LiMn$_2$O$_4$ electrodes observed during this study, the results from theoretical calculations proved very helpful for the interpretation.

2. Methodology

2.1. Theoretical calculations

The standard oxidation or reduction potential E^0 is usually calculated based on the difference of the standard free energies G^0 in solution of the species S and its oxidized form S^+. To transform this value into a potential value relative to the Li/Li$^+$ reference electrode, one has to subtract 1.46 V [41], thus [41,42]

$$E^0(S) = -\left[G^0(S) - G^0\left(S^+\right)\right]\Big/e - 1.46\,\mathrm{V} \qquad (1)$$

Note that the symbol S^+ is used here to denote the oxidized form of the molecule, independently of its charge. This method was applied to reduction potentials by Vollmer et al. [35,41] and further refined for efficient calculation of oxidation potentials by Wang et al. [42]. As has been noted by Wang et al. [42], the thermal contribution to the free energy difference is expected to be rather low; they found absolute values below 0.04 V over ten organic molecules. Furthermore, the calculation of the quantities needed turned out to be technically demanding. Consequently, it will be neglected in the following, and the standard free energy in solution without thermal

contribution constitutes the basis of the oxidation potentials according to Eq. (1); for details see literature [42].

Although today's computational power enables explicit simulations of large molecular systems, calculating solvation energies on the basis of an explicit representation of a large number of solvent molecules is still not feasible when aiming at a study comparing several additives. Instead of an atomistic resolution of the solvent molecules, solvation models as commonly implemented in the standard computational chemistry software packages can be used. One of these is the polarizable continuum model (PCM) [43], in which the solute is described by spheres of certain radii centered at the sites of the atomic cores within the molecule. These spheres form a cavity which is used to calculate the interactions of the molecule with the surrounding solvent, where the latter is taken into account e.g. by its dielectric constant and the molecule size. The PCM flavor used for this study was the conductor PCM (C-PCM) [44,45] model.

The calculations reported here were performed using the GAMESS [46,47] computational chemistry package. All illustrations of molecules and orbitals presented were produced using the MacMolPlt [48] program. The molecule geometries in the reduced and oxidized state were first optimized in vacuum on the HF/6-31G(d,p) level followed by a DFT optimization employing the B3LYP [49–52] hybrid functional, the PCM model and the same basis set. The final free energy values were obtained using a larger basis set including diffuse functions; so one more optimization run was performed at the B3LYP/6-311++G(d,p) level to allow for a proper description of the electron density further away from the atomic cores which is especially important for anionic species. Although the solvent employed in the experiments here (1 M LiPF$_6$ in EC:DMC (1:1 by wt.)) differs from the one described by Wang et al. (0.7 M LiBOB in EC:PC:DMC:DEC (1:1:2:2) [42]), the PCM parameters proposed by these authors proved to be suitable also for the description of our base electrolyte. Performing a sensitivity analysis, Wang et al. showed that the calculated oxidation potentials are quite insensitive to the solvent radius and the dielectric constant chosen [42]. Furthermore, comparing test calculations on molecules described in literature to experiments in our lab resulted in a satisfactory agreement of calculated and measured oxidation potentials. Consequently, a dielectric constant of 60.0 and a solvent radius of 5.0 Å were used for all calculations described below. To assign partial charges and spin population values to the atoms, the Mulliken [53] and Löwdin [54] population analysis methods were employed.

2.2. Experimental

The salicylato-borates were synthesized by the reaction of boric acid with two equivalents of ligand (salicylic acid or derivative) and one equivalent of LiOH or half an equivalent of Li$_2$CO$_3$, as shown in the reaction scheme in Fig. 2. The reaction of the components proceeded in an inert hydrocarbon solvent such as octane, while the reaction water was removed by azeotropic distillation. The reaction product was filtered, washed with hexane, and dried at 180 °C in a vacuum oven. The reaction yield was close to the theoretical value. The synthesized compounds listed in Table 1 were initially characterized by multinuclear NMR measurements (Avance DPX 250 from Bruker with 5 mm PABBO BB-1H/D Z-GRD) and were then subjected to thermogravimetric analysis (TGA) (NETZSCH TG 209 F1, under Ar-flow).

The ^{11}B-NMR data reflect the relative changes of the electron density around the central boron atom caused by the differently substituted ligands. According to the individual electron-withdrawing effects of these ligands the ^{11}B peaks are expected to shift in the following ascending order: dimethyl < unsubstituted <
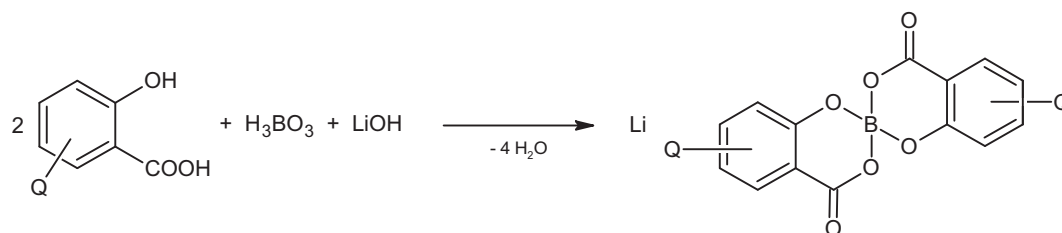
Fig. 2. Reaction scheme for the synthesis of lithium salicylato-borates.

Br < Cl < Di-Cl ∼ F. However, as explicitly seen, no considerable change is observable between the substituted bis(salicylato)borate derivatives. This is probably due to the fact that the positions of the ligands are far from the central boron atom and its electron cloud, and that therefore their influence remains insignificant. In contrast, oxalato moieties lead to a significant shift of the ^{11}B-NMR peaks to low field. By exchanging one oxalato against a salicylato group (from LiBOB to LiSOB) a significant increase of shielding (i.e. a high field shift of about 2 ppm) is observed. The oxalato ligand is more electron withdrawing (−I effect) as compared to the salicylato ligand. Thus a rough prediction can be made for the electron density on boron: LiBSB > LiSOB > LiBOB [32]. Beside ^{11}B-NMR data, Table 1 lists thermal stabilities of the synthesized chelato-borates. The decomposition generally starts at >250 °C and peaks at >320 °C. Especially the bis(salicylato) compounds exhibit an unusually high thermal stability.

The base electrolyte used in this study was LiPF$_6$ (Merck) in a mixture of ethylene carbonate (EC) and dimethyl carbonate (DMC) (1:1 by wt.) (Ube Industries). Lithium chelato-borates (LiBOB, LiSOB, LiBSB, LiBMSB, LiBFSB, LiBClSB, LiBBrSB, and LiBCl$_2$SB) were added to the base electrolyte at a concentration of 0.1 M. All electrolyte mixtures were prepared in an argon-filled glove box.

LiMn$_2$O$_4$ was used as active material for the positive electrode. A cathode slurry was prepared from 82 wt% active material, 10 wt% carbon black (SuperP Li, Timcal), 8 wt% polyvinylidene fluoride (PVdF, Solef 6020, Solvay Solexis) and N-methylpyrrolidone (NMP, Honeywell) as solvent and coated onto Al foil as current collector. Graphite (MAGD, Hitachi Chemical Company) was used as active material for the negative electrode. A slurry was prepared from 92 wt% graphite, 8 wt% PVdF and NMP and spread onto a Cu foil. The electrodes were dried at 130 °C in dynamic vacuum over night.

T-type three-electrode half cells were assembled using LiMn$_2$O$_4$ or graphite working electrodes and metallic Li counter and reference electrodes. Three sheets of borosilicate glass fiber separator (GF/A, Whatman International) were used and soaked with the chelato-borate containing electrolytes. The geometric area of the electrodes was 1.13 cm^2 and the typical loading of active materials was in the range of 3–4 mg. Electrochemical measurements were

Table 1
Analytical data for lithium chelato-borates.

Lithium chelato-borate	δ^{11}B (ppm) d$_6$-DMSO solution	Thermogravimetric analysis (°C)	
		Start	Peak
LiBOB	7.7 [33]	300	370
LiSOB	5.6 [33]	250	327
LiBSB	3.9	340	433
LiBMSB	4.0	320	417
LiBFSB	3.9	ca. 340	469
LiBClSB	3.8	480	508
LiBBrSB	3.7	ca. 320	ca. 430
LiBCl$_2$SB	3.7	ca. 330	458

performed at room temperature using a VMP Electrochemical Workstation from Princeton Applied Research/Biologic. CV measurements were performed at a scan rate of 0.1 mV s^{-1} in the potential ranges indicated in the text, starting from open circuit voltage (OCV).

3. Results and discussion

3.1. Theoretical calculations

Even though LiBOB has been extensively studied with regard to its use both as electrolyte salt and as additive for quite some time, the value of the oxidation potential seems still somehow unclear, and differing values have been proposed based on experimental and computational studies. To the best of our knowledge the lower boundary has been established at 4.5 V vs. Li/Li$^+$ [55]. Thus, investigating the oxidation behavior of this compound was chosen as a starting point and reference for the study focused on salicylato-borates presented in this communication. As the salts investigated here are expected to be present in the dissociated form when dissolved in the electrolyte, the oxidation behavior was studied taking into account only the corresponding anions, i.e. the bis(oxalato) borate (BOB$^-$) anion in the case of LiBOB. The optimized molecular geometries of both BOB$^-$ and the BOB• radical are shown in Fig. 3 together with an illustration of the corresponding highest occupied molecular orbital (HOMO) and lowest unoccupied molecular orbital (LUMO), respectively. As during oxidation of a closed-shell species one electron is removed from the HOMO leaving a singly-occupied orbital in the radical formed, the properties of these orbitals greatly influence the oxidation behavior.

The calculated oxidation potential based on the difference of the PCM free energy values in solution amounts to 5.98 V obtained using B3LYP/6-311++G(d,p). In contrast to the full optimization of both the anion and radical structure as employed here, Johansson [56] uses the concept of the vertical electronic energy difference ΔE_v according to the Franck–Condon principle, i.e. the electronic energy of the oxidized species is obtained by performing a single-point calculation on the basis of the unchanged molecular structure of the reduced form. By studying 12 anions and comparing several computational methods, he shows that employing good-quality DFT functionals and basis sets, the correlation of ΔE_v to the oxidation potential is clear and remarkably better than the correlation obtained by just using the energy level of the HOMO. Furthermore, Johansson also uses a free energy correction, but rates the improvement thus reachable dubious [56]. To benchmark our methodology, we also calculated ΔE_v for BOB$^-$, which yielded a value of 4.71 V vs. Li/Li$^+$ in very good agreement to Johansson's value of 4.72 V vs. Li/Li$^+$ [56], thus demonstrating that in spite of using a slightly smaller basis set, included in a different software solution, the results are well comparable. Nevertheless, the experimental results found within the present study indicate that the oxidation potential of BOB$^-$ should be at least larger than 5.0 V vs. Li/Li$^+$ (cf. below). This supports the view that to obtain *absolute*
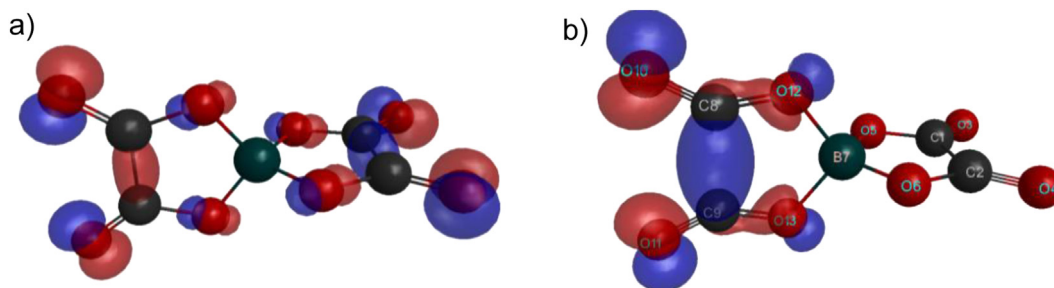
Fig. 3. Optimized molecular geometries for the (a) BOB⁻ anion and (b) BOB• radical, together with iso-surfaces illustrating shape and expansion of the relevant orbitals (a) HOMO of BOB⁻ and (b) LUMO of the BOB• radical.

potential values, either a correlation over several comparable molecules must be investigated or one has to rely on embedding the molecule into a proper solvent model as attempted here.

Investigation of the electronic structures of the anion and the radical reveals that the HOMO of the anion expands over practically the entire molecule, whereas the radical LUMO is restricted to one of the oxalato groups, cf. Fig. 3. Analyzing the atomic spin population furthermore shows that the unpaired spin is largely located at the C8, C9, O10, and O11 atoms. Thus, one can comprehend why the bond distance between C8 and C9 grows from 1.55 Å to 1.93 Å, whereas the bond order decreases from 0.76 to 0.39. Remarkably, the partial charge of the boron atom, both determined by the Mulliken and the Löwdin methods, hardly changes during oxidation. In fact − complying with the orbital picture shown in Fig. 3(b) − the loss of one electron charge occurs mainly at one of the oxalato groups. One might speculate that the observed ring cleavage may lead to a consecutive reaction involving CO_2 release, possibly also after a second oxidation step. This would render the whole oxidation process irreversible. But a substantiated investigation would require the calculation of several, possibly many reaction paths, which is beyond the scope of the present study.

Going to the next anion, the mixed salicylatooxalatoborate (SOB⁻), the primary question is, from which group the electron will be taken during oxidation − again from the oxalate, or rather from the aromatic structure. The optimized structures of the anion and the SOB• radical are shown in Fig. 4. The calculated oxidation potential for SOB⁻ is 4.75 V vs. Li/Li⁺, i.e. 1.25 V lower than that of BOB⁻, indicating that the reaction must be substantially different. Comparing the locations of the SOB⁻ HOMO (Fig. 4(a)) and the SOB• LUMO (Fig. 4(b)), it is very clear that both of them are located mainly at the aromatic ring and the alkoxy-oxygen (O12, cf. Fig. 4 for atom labels) of the salicylato group. This picture is also supported by the analysis of the atomic spin population and the partial charges in the molecule. Both the Mulliken and the Löwdin methods show in agreement that more than $0.8e$ of the charge removed during oxidation originate from the salicylato group. As in

the case of BOB⁻, the partial charge of the boron atom does not change significantly upon oxidation.

Regarding the molecule geometry, changes between the reduced and oxidized forms are rather minor. Comparing Fig. 4(a) and (b) one can see that in subfigure (a) double bonds are drawn between C4 and O6 and between C2 and O3, respectively, whereas single bonds are drawn in subfigure (b). On the other hand, a double bond appears between C11 and O12 in the oxidized molecule, where we find only a single bond drawn in the reduced structure. But this is just due to the fact that the corresponding bond distance is slightly higher or lower than the threshold value the program MacMolPlt [48] uses to discriminate single and double bonds, and so this effect should not be overrated.

Comparing the results for BOB⁻ and SOB⁻, it is clear that the salicylato group undergoes oxidation much easier than the oxalato group. Consequently, the behavior of the bis(salicylato)borate (BSB⁻) anions can be expected to resemble rather that of the SOB⁻ anion. Still, it has to be clarified whether the BSB⁻ compounds might feature a HOMO/LUMO shape which extends over both ligands allowing for a better delocalization of the unpaired electron, or if again just one of the groups donates nearly all of the charge.

The calculated oxidation potential of the BSB⁻ anion is found to be at 4.46 V vs. Li/Li⁺, that means even by 0.3 V lower than for SOB⁻. The shapes of the relevant HOMO and LUMO orbitals are shown in Fig. 5(a) and (b) together with the corresponding optimized structures of the anion and the radical. Again, both HOMO and LUMO are mainly located at one of the salicylato groups, although some contribution of the other group can be detected, especially in the case of the radical. (It should be noted that according to the atom labels, it appears that the LUMO occupies the other group compared to the main location of the HOMO. The reason for this is simply that within the anionic structure, both salicylato groups are equivalent, consequently there also exist two quasi-equivalent orbitals of highest energy, so it is just due to small numerical differences that one of them is labeled the HOMO. After oxidation, both groups are no longer equivalent, and apparently the electron has been taken from the other salicylato group in this case, but
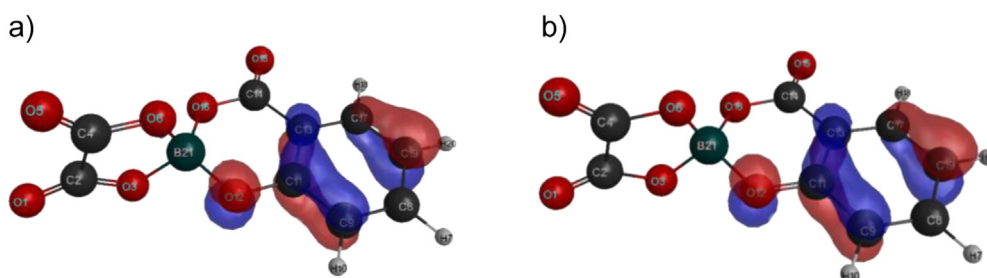

Fig. 4. Oxidation of salicylatooxalatoborate (SOB⁻), (a) anion structure and HOMO, (b) SOB• radical and LUMO.
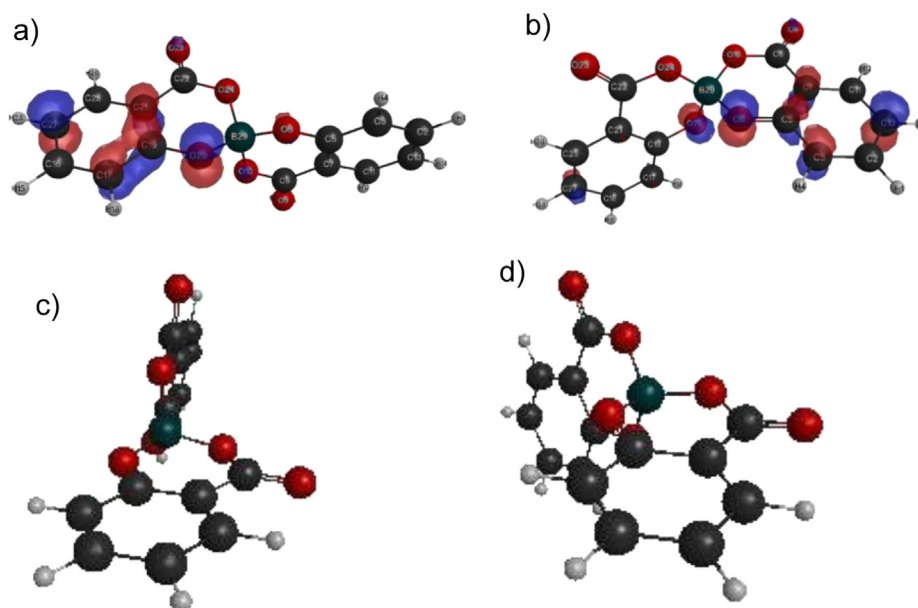
Fig. 5. Bis(salicylato)borate (BSB⁻), structure and orbital shape of the (a) BSB⁻ anion with HOMO, (b) BSB• radical with LUMO; to illustrate the structural changes during oxidation (c) and (d) feature a different viewpoint of the anion and radical, respectively.

there is no physical meaning to this.) So, to answer the question posed above, again the oxidation is mainly restricted to just one group. Analyzing the spin population gives a result in good agreement with the LUMO shape. Both the Mulliken and Löwdin methods show that a large share of the unpaired spin can be attributed to the C13, O6, and C3 atoms.

From Fig. 5(a) and (b) it becomes somehow clear that the molecule structure has changed upon oxidation, but this perspective is rather suitable for assessing the orbital structure. Thus the geometric structures before and after oxidation, respectively, are shown once more from a different viewpoint in subfigures (c) and (d) featuring the salicylato group in front at a fixed position and alignment. Here, it becomes clear that there are some changes in geometry which break the symmetry of the two salicylato groups and induce a rotation around the boron atom at the molecule center. Similar to the case of SOB⁻ the single bond between C5 and O6 becomes a double bond after oxidation. Again, this corresponds to rather minor changes in bond length and order; the corresponding bond order increases from 1.35 to 1.67.

To assess the influence of substitution at the aromatic rings of BSB⁻, a series of compounds connatural to BSB⁻ was chosen for further investigation. To cover both electron withdrawing and donating groups these include the mono halogen-substituted

bis(5-fluorosalicylato)borate (BFSB⁻), bis(5-chlorosalicylato)borate (BClSB⁻), bis(5-bromosalicylato)borate (BBrSB⁻), the di-halogen-substituted bis(3,5-dichlorosalicylato)borate (BCl₂SB⁻), and the mono alkyl-substituted bis(3-methylsalicylato)borate (BMSB⁻).

Concerning the oxidation potentials, the observed trends largely comply with what should be expected. In Table 2 the obtained potential values are summarized and compared to their experimental counterparts. Taking the value of 4.46 V vs. Li/Li⁺ obtained for BSB⁻ as a reference, the oxidation stability is lowered in the case of BMSB⁻ (4.33 V vs. Li/Li⁺). Removing one electron is facilitated by the electron donating inductive and mesomeric effects (+I, +M) of the methyl group in this case. For halogen substituents usually an electron-withdrawing inductive effect (−I) superimposed by a positive mesomeric effect (+M), which depends on the electronegativity of the respective element, is described in organic chemistry textbooks. Turning to the mono halogen-substituted compounds investigated here, no really clear trend can be observed. For BFSB⁻ we find a very weak electron-withdrawing effect (4.49 V vs. Li/Li⁺), but surprisingly for BClSB⁻ it appears stronger (4.57 V vs. Li/Li⁺). For BBrSB⁻ we find as expected only a tiny effect, if significant at all (4.47 V vs. Li/Li⁺). (It should be noted that the oxidation potential of BBrSB⁻ was calculated using the smaller 6-31G++(d,p) basis set as the 6-311G++(d,p) basis is not

Table 2
Summary of reduction and oxidation potentials obtained from experimental studies and theoretical calculations.

Anion	Reduction potential (exp.) (V) vs. Li/Li⁺	1st oxidation potential (exp.) (V) vs. Li/Li⁺	1st oxidation potential (theor.) (V) vs. Li/Li⁺	2nd oxidation potential (theor.) (V) vs. Li/Li⁺
BOB⁻	1.71[a]		5.98	
SOB⁻	1.60 and 1.02[a]	4.51, 4.75[b]	4.75	6.37
BSB⁻	0.97[a]	4.46[b]	4.46	5.47
BMSB⁻	0.89[a]	4.36[b]	4.33	
BFSB⁻	1.45, 1.12, 0.75[a]	4.4, 4.65[a]	4.49	5.48
BClSB⁻	1.65, 1.30, 0.90[a]	Onset 4.50[a]	4.57	
BCl₂SB⁻	1.35[a]	4.55 (shoulder), 4.80[a]	4.62	
BBrSB⁻	1.45, 1.30, 0.90[a]	4.47, 4.70[a]	4.47[c]	

[a] 0.1 M in 1 M LiPF₆/EC:DMC (1:1 by wt.).
[b] 0.1 M in EC:DMC (1:1 by wt.).
[c] Calculated using the 6-31G++(d,p) basis set.

available for Br.) Finally, substituting with two chlorine atoms per aromatic ring results in the highest oxidation stability observed for the bis(salicylato)borates investigated here: BCl_2SB^- yields 4.62 V vs. Li/Li$^+$. Overall, the influence of substitution at the aromatic rings on the oxidation potential appears rather slight, though of course 4.62 V vs. Li/Li$^+$ may make sense in the case of specific battery chemistry with cathode materials working up to 4.2 V vs. Li/Li$^+$, for which 4.33 V vs. Li/Li$^+$ is still too low.

Concerning changes in the structure during oxidation, $BMSB^-$ shows an inner-molecular rotation alike to BSB^-. A similar effect, though less pronounced, can be observed in the case of the mono halogen-substituted compounds, whereas for BCl_2SB^-, there are no apparent structural differences between anion and radical. The overall structural behavior of the molecules during oxidation may be influenced by a combination of electronic, size and steric effects, the latter especially depending on the particular site of substitution. As all optimization runs this discussion refers to were performed using the PCM model, one should be aware that the actual behavior concerning this feature may also be influenced by the real shape of and specific interactions with the solvent molecules. In contrast, the oxidation potential this study is focused on can be expected to be rather insensitive to this effect.

3.2. Experimental characterization

3.2.1. Reduction stability of lithium chelato-borates

The reduction stability of the lithium chelato-borates has been characterized by CV at graphite electrodes between 1.5 and 0.02 V vs. Li/Li$^+$ at a scan rate of 0.1 mV s^{-1} in 1 M LiPF$_6$/EC:DMC (1:1 by wt.) (a) without additive, (b) with 0.1 M LiBOB, (c) with 0.1 M LiSOB, (d) with 0.1 M LiBSB, and (e) with 0.1 M LiBMSB. The results are presented in Fig. 6 and in enlarged detail in Fig. 7. The results obtained for the additive-free electrolyte are used as reference (Fig. 6(a)). Lithium intercalation occurs below 0.5 V vs. Li/Li$^+$ and gives rise to the reversible formation of staging compounds of graphite [57], marked as "a", "b", "c", and "d". Besides, an additional reduction wave is detected around 0.85 V vs. Li/Li$^+$ in the course of the 1st cathodic scan, which is ascribed to the formation of a SEI.

In the presence of LiBOB salt, Fig. 6(b), a characteristic reduction signal is observed at around 1.75 V vs. Li/Li$^+$, which can be related to the reduction of LiBOB itself or of some LiBOB-related intrinsic impurity [9,20,58]. A primary SEI film starts to form at this potential and later at lower potentials this film undergoes subsequent modifications and stabilizes [9,13]. Furthermore, in the LiBOB containing electrolyte the Li intercalation peaks experience some broadening and peak "b" is no longer resolved. The broader peaks and corresponding lower current values recorded in the LiBOB containing electrolyte indicate slightly worsened electrode kinetics as compared to the reference.

The CV curves of graphite in the LiBSB and LiBMSB containing electrolytes (Fig. 6(d) and (e)) exhibit no significant difference. There is only a slight shift in the reduction potential of LiBMSB due to the electron pushing effect (+I and +M effects) of the methyl group (see Fig. 7). LiSOB (Fig. 6(c)) shows a combined electrochemical behavior of LiBOB and LiBSB. Two reduction signals are detected at potentials of 1.6 V and 1.0 V vs. Li/Li$^+$, which are ascribed to the reduction of the oxalato and the salicylato moieties, respectively, since they occur at similar potentials as the reduction peaks of LiBOB and LiBSB.

Fig. 8 presents the CV curves of the graphite electrodes in halogenated bis(salicylato)-borates and Fig. 9 shows an enlarged view of the 1st cycles. Similar to the non-halogenated chelato-borates mentioned above, the reduction of the halogenated salicylato-borates begins at potentials below 2 V vs. Li/Li$^+$. Presumably, in the course of the 1st half cycles, the reduction of the halogenated
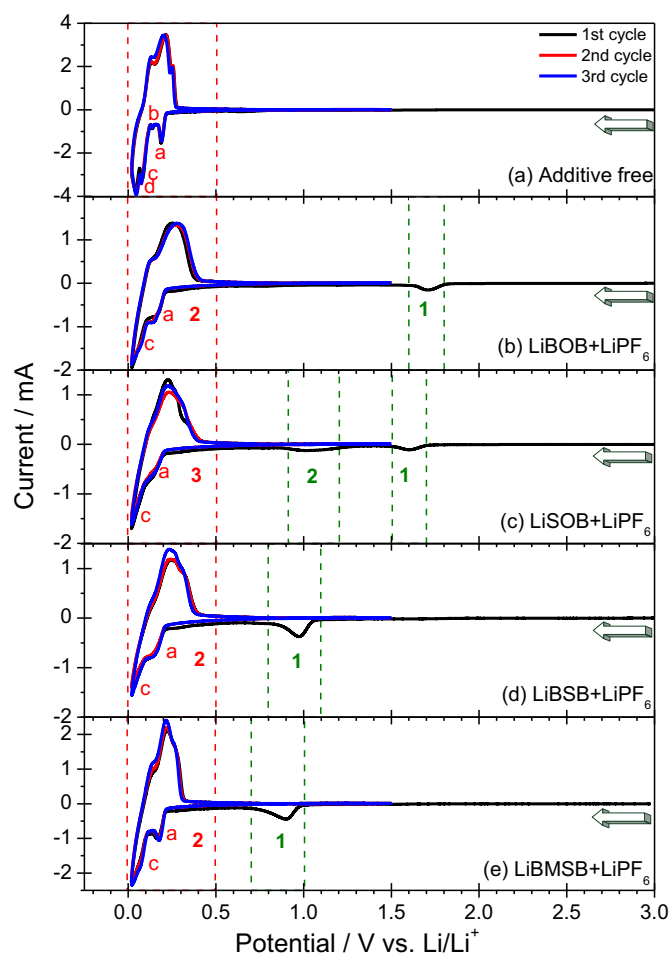

Fig. 6. CV curves of graphite cycled in 0.1 M non-halogenated lithium borate in 1 M LiPF$_6$/EC:DMC (1:1 by wt.) at a scan rate of 0.1 mV s^{-1}.

salicylato-borate anions and the reduction of some impurities in the sample or the reduction of electrolyte constituents may occur consecutively, and this is most likely responsible for the serial reduction peaks observed in the CV curves. Three reduction peaks are obtained for LiBFSB (Fig. 8(a)) at 1.45 V, 1.12 V, and 0.75 V vs. Li/Li$^+$. The intensity of the 1st peak is lower than that of the 2nd one and could
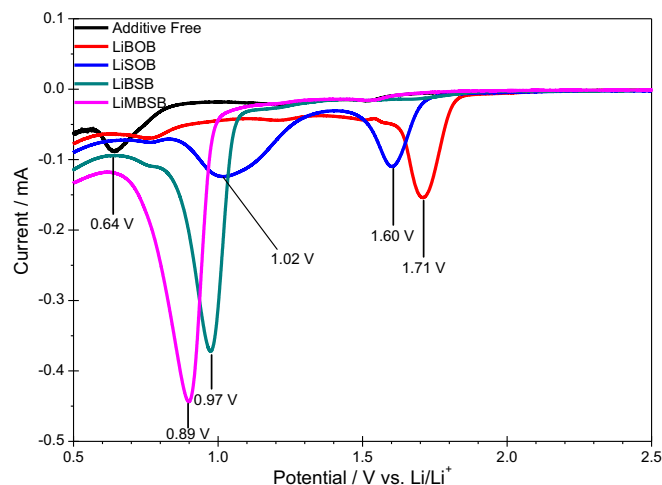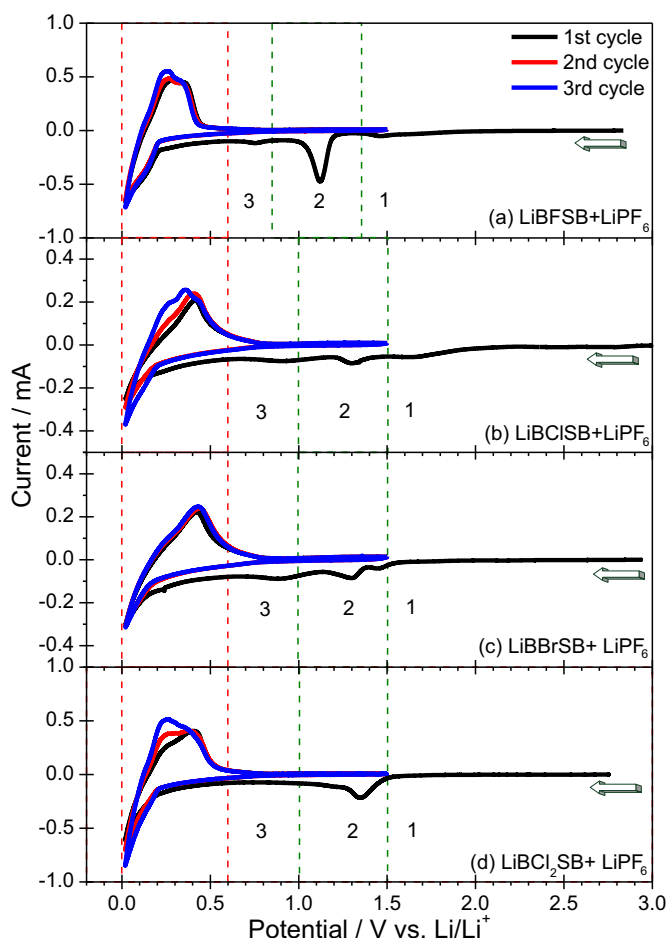

Fig. 7. Enlarged detail of Fig. 6.

Fig. 8. CV curves of graphite cycled in 0.1 M halogenated lithium borate in 1 M LiPF$_6$/EC:DMC (1:1 by wt.) at a scan rate of 0.1 mV s^{-1}.

be due to the reduction of impurities. The position of the 2nd peak is consistent with the observed reduction signal of the BSB$^-$ anion (Fig. 6(d)), and is therefore attributed to the reduction of BFSB$^-$ – probably together with the formation of a primary SEI (as in the case of BOB$^-$). The 3rd peak appearing at 0.74 V vs. Li/Li$^+$ may be related to the reduction of some solvent species or to a further reduction and

Fig. 9. Enlarged detail of Fig. 8.

reorganization of the primary SEI film. Similarly, three reduction peaks are detected for LiBClSB (Fig. 8(b)) at 1.65, 1.30, and 0.90 V vs. Li/Li$^+$. The intensities of these peaks are much lower as compared to those of LiBFSB. A similar electrochemical performance is also detected for LiBBrSB (Fig. 8(c)). The most distinctive reduction behavior is noticed for BCl$_2$SB$^-$ (Fig. 8(d)). No irreversible reduction peak is recorded higher than 1.35 V vs. Li/Li$^+$ and lower than 1.00 V vs. Li/Li$^+$. The peak detected at 1.35 V vs. Li/Li$^+$ implies that the SEI is mainly formed at this potential and the surface film does not allow other species to undergo reduction.

In order to quantify the amount of charge irreversibly consumed by the additives, the CV curves shown in Figs. 6 and 8 have been integrated in several potential regions: the potential range for the 1st area is selected such that it comprises the irreversible reduction peaks of the additives, the 2nd area ranges from 0.5 V to 0.02 V vs. Li/Li$^+$, the 3rd area ranges from 0.02 V vs. Li/Li$^+$ to the zero crossing potential (ZCP), and finally the 4th area is integrated from the ZCP to 1.5 V vs. Li/Li$^+$. The sum of the capacity values obtained for areas 1 + 2 + 3 describes the total charge capacity and the value found for the 4th area denotes the total discharge capacity. The irreversible capacities due to the borate reduction peaks (area 1) have been normalized to the first total charge capacity and are listed in Table 3. It is evident that the irreversible capacities are higher and the coulombic efficiencies are lower for the halogenated salicylato-borates than for the non-halogenated ones, which indicates a poor cycling efficiency of graphite in the presence of these additives.

Generally the differences in coulombic efficiency are ascribed to differences in the electrolyte reduction and SEI formation behavior, and to the possible presence of impurities introduced with the salts. The SEI chemistry depends on the electrolyte composition. Xu et al. [13,58–60] reported that the SEI formed in the presence of LiBOB mainly contains boron species. Boron is present as 3-fold coordinated borate, i.e. the boron symmetry changes from BO$_4$ to BO$_3$ during the reduction, and evidently BO$_3$-containing polymeric species are the essence of the SEI. As for the SEI formed in the presence of LiBSB, Aurbach et al. [27] reported that salicylic acid derivatives, namely carboxylates (–COOLi), which are formed upon reduction of BSB$^-$ via B–O bonds, are the main constituent of the SEI. In principle, similar decomposition products can be expected for the substituted salicylato-borates – with the difference that instead of the phenyl ring a substituted phenyl ring is present. However, due to shifts in the reduction potential of the substituted salicylato-borates, the relative composition of the SEI may differ. Assuming that SEI formation is a competition between several reactions, including reduction of salts and solvents and reactions between electrode surface groups and salts and solvents, the SEI may be enriched in products from reduction reactions which occur earlier (i.e. at higher potential) and/or faster. Hence a shift of the reduction potential of the salicylato-borate toward higher or lower values may increase or decrease the relative amount of their decomposition products in the SEI.

3.2.2. Oxidation stability of lithium chelato-borates

The anodic stability limits of the non-halogenated and halogenated chelato-borates have been estimated with LiMn$_2$O$_4$ electrodes using CV between 3.0 and 5.0 vs. Li/Li$^+$ at a scan rate of 0.1 mV s^{-1}. The CV curves and the enlarged views of the 1st anodic half cycles can be viewed in Figs. 10–14. The CV curve of the reference electrolyte (1M LiPF$_6$/EC:DMC (1:1 by wt.), Fig. 10(a)) exhibits the characteristic Li$^+$ deinsertion/insertion double peaks of LiMn$_2$O$_4$. The slight increase in current above 4.9 V vs. Li/Li$^+$ is attributed to the onset of decomposition of the base electrolyte. In the LiBOB containing electrolyte (Fig. 10(b)), no significant differences are observed as compared to the additive-free electrolyte and that Li$^+$ deinsertion/insertion remains unobstructed. The slight
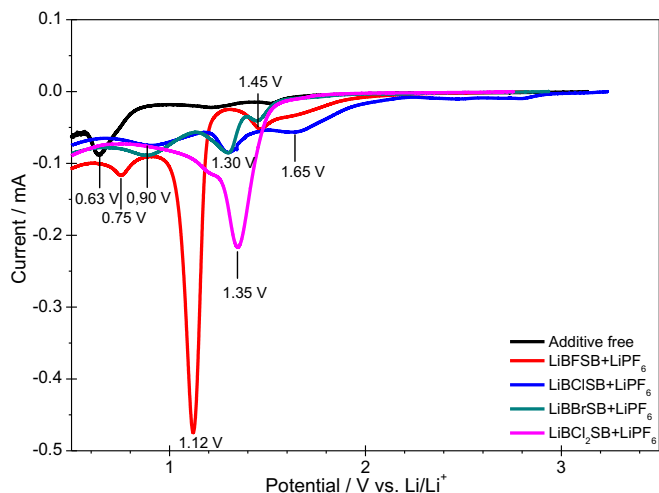
Table 3
1st cycle potential and capacity data for lithium chelato-borates (derived from Figs. 6 and 8).

Additive	1st peak (for LiSOB 1st and 2nd)		2nd + 3rd peaks		Total charge capacity (1 + 2 + 3) (mAh cm^{-2})	Total discharge capacity 4th (mAh cm^{-2})	Irreversible capacity[a] (%)	Coulombic efficiency (%)
	Potential range (V) vs. Li/Li$^+$	Capacity (mAh cm^{-2})	Potential range (V) vs. Li/Li$^+$	Capacity (mAh cm^{-2})				
None	1.5−0.5	0.084	0.5−0.02 and 0.02-zpc	1.062	1.147	1.066	8.00	92.97
LiBOB	1.8−1.5	0.084		0.818	0.902	0.648	9.30	73.15
LiSOB	1.7−1.6	0.061		0.658	0.852	0.554	22.74	65.10
	1.6−0.8	0.132						
LiBSB	1.1−0.8	0.212		0.661	0.873	0.544	24.31	62.31
LiBMSB	1.1−0.8	0.265		0.857	1.122	0.748	23.64	66.66
LiBFSB	OCV-0.5	0.278		0.404	0.683	0.274	40.70	40.11
LiBClSB	OCV-0.5	0.177		0.155	0.332	0.080	53.31	24.00
LiBBrSB	OCV-0.5	0.144		0.261	0.405	0.154	35.55	38.00
LiBCl$_2$SB	OCV-0.5	0.223		0.358	0.557	0.262	40.03	47.03

[a] Irreversible capacity (%) is normalized to the total charge capacity of the graphite electrodes.

differences in peak potentials and currents may be caused by the effect of LiBOB on the viscosity (η) and conductivity of the electrolyte ($\eta_{ref} = 3.40$ mPa s and $\eta_{LiBOB} = 4.45$ mPa s). Furthermore, recently LiBOB has been reported to form a surface film at the cathode [61,62], which may be an additional explanation for the relative changes in CV curves of LiMn$_2$O$_4$ in the presence of LiBOB.

For 0.1 M LiSOB, LiBSB, and LiBMSB in 1 M LiPF$_6$/EC:DMC (1:1 by wt.) broad oxidation waves are observed peaking at potentials between 4.58 and 4.73 V vs. Li/Li$^+$ (Fig. 11). In the case of LiBSB

and LiBMSB these values are higher than the calculated oxidation potentials. A closer inspection shows minor features (peaks or shoulders) at already lower potentials. In Fig. 12 the experiment was repeated with 0.1 M borate in EC:DMC (1:1 by wt.) without LiPF$_6$. Interestingly, for LiBSB and LiBMSB oxidation potentials of 4.46 and 4.36 V vs. Li/Li$^+$ are obtained now, which perfectly match the calculated values (Table 2). For LiSOB two oxidation peaks are resolved, where the peak at higher potential is close to the calculated value and could resemble oxidation of SOB$^-$. The origin of the lower potential peak is unclear. The differences in the presence and absence of LiPF$_6$ might be due to concentration effects (due to the high amount of Li in the presence of 1 M LiPF$_6$) or to cooperative effects between the borate and PF$_6^-$ anions.

Also the anodic behavior of the halogenated bis(salicylato) borates in 1 M LiPF$_6$/EC:DMC (1:1 by wt.) is complex (Figs. 13 and 14). Two (or more) oxidation peaks are observed in addition to the LiMn$_2$O$_4$ peaks. The onset of oxidation, visible as small peaks or shoulders in the CV curves, is between 4.3 and 4.6 V vs. Li/Li$^+$. This region is followed by stronger oxidation peaks between 4.5 and 4.9 V vs. Li/Li$^+$. Based on the electrochemical results alone an exact interpretation of the observed oxidation peaks is difficult. The calculated first oxidation potentials are closer to the experimentally observed oxidation onset potentials than to the second (stronger) oxidation peaks. The oxidation onset potentials decrease in the order LiBCl$_2$SB > LiBClSB > LiBBrSB > LiBFSB, which is the same sequence as observed on glassy carbon electrodes by Nanbu et al. [30]. The second oxidation potentials were calculated to be higher
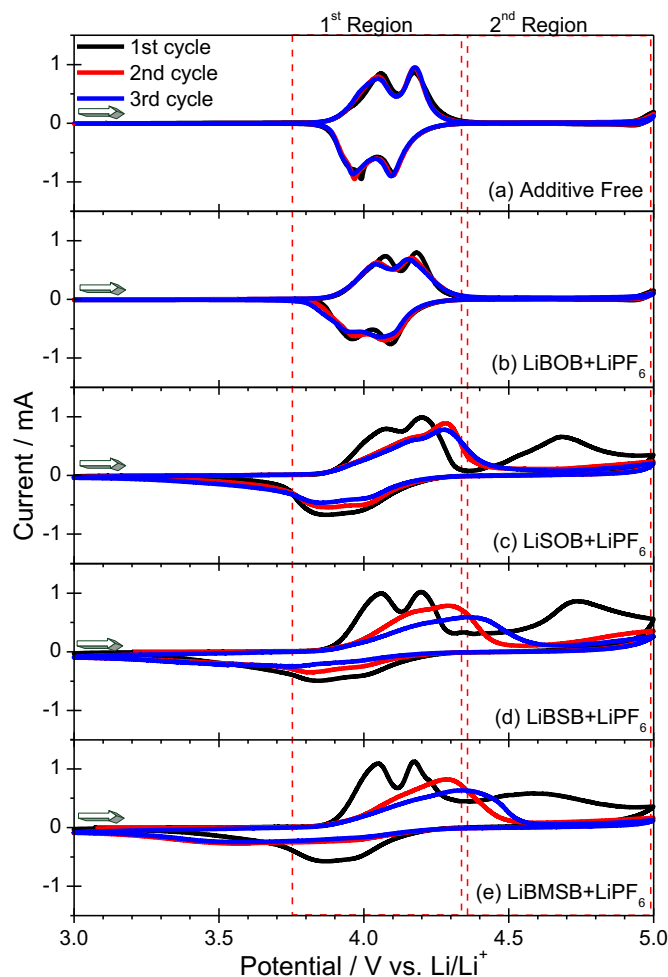

Fig. 10. CV curves of LMn$_2$O$_4$ electrodes cycled in 0.1 M non-halogenated lithium borate in 1 M LiPF$_6$/EC:DMC (1:1 by wt.) at a scan rate of 0.1 mV s^{-1}.
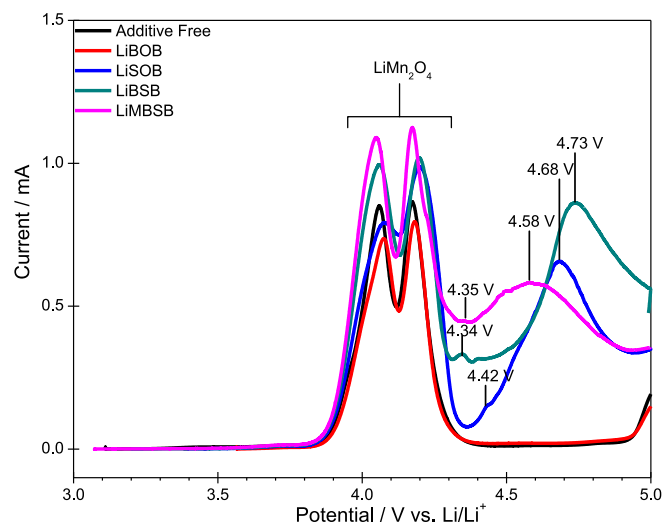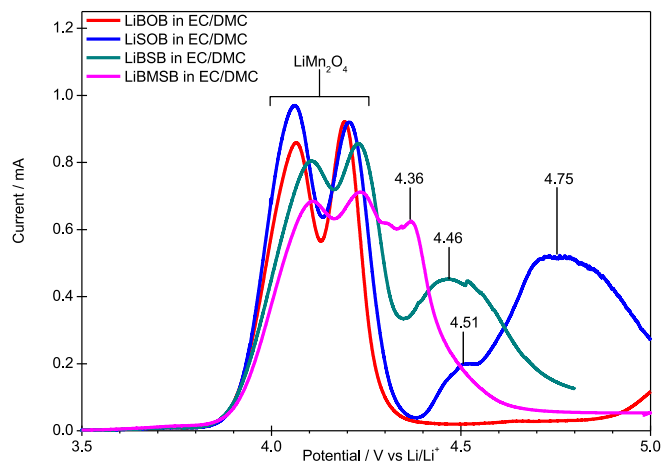

Fig. 11. Enlarged detail of Fig. 10.

Fig. 12. CV curves of $LiMn_2O_4$ electrodes cycled in 0.1 M lithium borate in EC/DMC (1:1 by wt.) *without* $LiPF_6$ at a scan rate of 0.1 mV s^{-1}.

than 5 V vs. Li/Li$^+$. Therefore it is unlikely that the second (stronger) oxidation peaks observed in the CV curves are due to a second oxidation of the bis(salicylato)borate molecules. They might instead reflect secondary oxidative decomposition reactions of the oxidized bis(salicylato)borates or reactions between the oxidized borates and the $LiMn_2O_4$ electrodes.

For all bis(salicylato)borates the back reduction scan and the subsequent cycles (Figs. 10 and 13) show a sluggish behavior, and
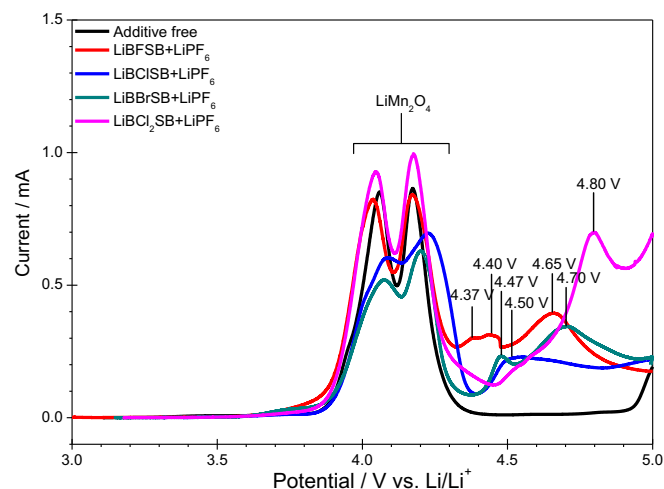

Fig. 13. CV curves of $LiMn_2O_4$ electrodes cycled in 0.1 M halogenated lithium borate in 1 M $LiPF_6$/EC:DMC (1:1 by wt.) at a scan rate of 0.1 mV s^{-1}.

Fig. 14. Enlarged detail of Fig. 13.

the typical $LiMn_2O_4$ double peaks partly or fully disappear. Such behavior may be explained by the formation of surface films (from borate decomposition products) and progressing passivation of the $LiMn_2O_4$ electrode, as has been proposed for benzenediolato-borates [21–25], LiBOB [61,62] and LiBSB [27]. For LiBOB, it has been shown that the film on a $Li_{1.17}Mn_{0.58}Ni_{0.25}O_2$ electrode is dominated by borate species (beside very small amounts of poly-ethylene carbonate and LiF) [61]. For a $LiNi_{0.5}Mn_{0.5}O_2$ electrode it has been proposed that a Mn^{2+}-containing oxalate-borate surface layer is formed on the electrode surface, which suppresses Mn dissolution [62]. For LiBSB it has been proposed that the passivation film contains species with ester and/or anhydride groups [27]. Clearly, further analytical investigations are needed to get a final picture of the occurring oxidation processes.

3.3. Comparison of experimental and theoretical results

The experimental results derived from the CV curves and the theoretical values calculated as presented above are summarized in Table 2 for comparison. No experimental oxidation potential has been observed for the BOB$^-$ anion within the investigated potential range (which was limited to 5 V vs. Li/Li$^+$ and thus far below the calculated oxidation value of 5.98 V vs. Li/Li$^+$). For the other borates, a good agreement between the experimental and calculated values has been found. For instance, a lower oxidation stability is exper-imentally observed for BMSB$^-$ as compared to BSB$^-$, and the same decreasing trend has been predicted by the theoretical calculations. The same is true for the halogenated salicylato-borates, where both experimentally and theoretically increased oxidations stabilities are found. The highest oxidation potential is reported in both cases for the BCl$_2$SB$^-$ anion.

4. Conclusions

In this paper several unsubstituted and substituted lithium chelato-borates have been investigated as electrolyte additives. It has been found that these lithium salts undergo reduction at graphite electrodes below 1.8 V vs. Li/Li$^+$ and oxidation at $LiMn_2O_4$ electrodes above 4.3 V vs. Li/Li$^+$. The shapes of CV curves of the graphite electrodes reflect the main changes in the presence of these additives. The kinetics of the graphite electrodes change due to the alteration of the Li$^+$ mobility in the SEI, the chemical nature of which is determined by the contribution of the additives. Especially in the halogenated bis(salicylato)borate containing
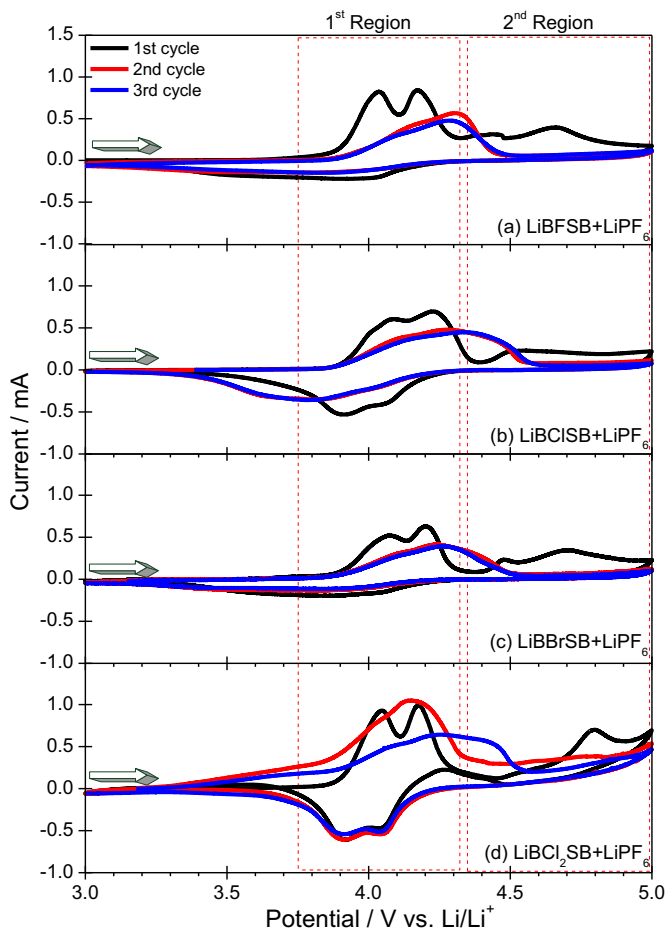
electrolytes the 1st cycle coulombic efficiencies of the graphite electrodes and the lithium insertion rate are strongly decreased after the SEI formation, which leads to significantly lower current values as compared to the additive-free reference electrolyte.

The oxidation of the salicylato-borates on the LiMn$_2$O$_4$ surface occurs irreversibly and results in the formation of passivating surface films. The further lithiation and delithiation peaks of the cathode become increasingly sluggish due to the hindered Li$^+$ deinsertion/insertion. Concerning the oxidation process of these additives, the corresponding potential values can be predicted by theoretical calculations. It has been shown that the large gap between the very high oxidation potential of LiBOB and the lower values found for LiSOB and LiBSB is due to the different groups which donate the electron: once a salicylato group is present, the electron will be taken from the latter, which results in the lower oxidation potential values observed; thereby, the aromatic π-electron system plays an important role to delocalize the single electron. Nevertheless, always mainly just one of the oxalato or salicylato groups is involved in the oxidation process and no significant delocalization of the HOMO or LUMO over the whole molecule could be observed for the bis(salicylato)borates.

Among the investigated borates, LiBOB showed the best stability and performance (at least when used as pure salt or as additive at concentration levels used in this work).

Acknowledgments

References

[1] R.M. Dell, Solid State Ionics 134 (2000) 139.
[2] B. Scrosati, J. Garche, J. Power Sourc. 195 (2010) 2419.
[3] M. Armand, J.-M. Tarascon, Nature 451 (2008) 652.
[4] A.G. Ritchie, J. Power Sourc. 136 (2004) 285.
[5] S.S. Zhang, J. Power Sourc. 162 (2006) 1379.
[6] K. Xu, S. Zhang, T.R. Jow, W. Xu, C.A. Angell, Electrochem. Solid State Lett. 5 (2002) A26.
[7] J.-C. Panitz, U. Wietelmann, M. Scholl, DE 10111410C (2002), US 7226704B (2007).
[8] J.-C. Panitz, A. Pötschke, R. Dietz, U. Wietelmann, EP 1726061B, CN 1957498B (2010), 2008.
[9] M. Wachtler, M. Wohlfahrt-Mehrens, S. Ströbele, J.-C. Panitz, U. Wietelmann, J. Appl. Electrochem. 36 (2006) 1199.
[10] D.-T. Shieh, P.-H. Hsieh, M.-H. Yang, J. Power Sourc. 174 (2007) 663.
[11] C. Täubert, M. Fleischhammer, M. Wohlfahrt-Mehrens, U. Wietelmann, T. Buhrmester, J. Electrochem. Soc. 157 (2010) A721.
[12] K. Xu, S. Zhang, T.R. Jow, Electrochem. Solid State Lett. 6 (2003) A117.
[13] K. Xu, U. Lee, S.S. Zhang, T.R. Jow, J. Electrochem. Soc. 151 (2004) A2106.
[14] K. Xu, S. Zhang, R. Jow, J. Power Sourc. 143 (2005) 197.
[15] K. Xu, S. Zhang, T.R. Jow, Electrochem. Solid State Lett. 6 (2005) A365.
[16] B.-T. Yu, W.-H. Qiu, F.-S. Li, L. Cheng, J. Power Sourc. 166 (2007) 499.
[17] J. Jiang, J.R. Dahn, Electrochem. Solid State Lett. 6 (2003) A180.
[18] S. Wang, W. Qiu, T. Li, B. Yu, H. Zhao, Int. J. Electrochem. Sci. 1 (2006) 250.
[19] D.P. Abraham, M.M. Furczon, S.-H. Kang, D.W. Dees, A.N. Jansen, J. Power Sourc. 180 (2008) 612.
[20] J.-C. Panitz, U. Wietelmann, M. Wachtler, S. Ströbele, M. Wohlfahrt-Mehrens, J. Power Sourc. 153 (2006) 396.
[21] J. Barthel, M. Wühr, R. Buestrich, H.J. Gores, J. Electrochem. Soc. 142 (1995) 2527.
[22] J. Barthel, B. Buestrich, E. Carl, H.J. Gores, J. Electrochem. Soc. 143 (1996) 3565.
[23] J. Barthel, R. Buestrich, E. Carl, H.J. Gores, J. Electrochem. Soc. 143 (1996) 3572.
[24] J. Barthel, R. Buestrich, H.J. Gores, M. Schmidt, M. Wühr, J. Electrochem. Soc. 144 (1997) 3866.
[25] J. Barthel, A. Schmid, H.J. Gores, J. Electrochem. Soc. 147 (2000) 21.
[26] M. Wühr, DE 43 16 104 A1, 1994.
[27] D. Aurbach, J.S. Gnanaraj, W. Geissler, M. Schmidt, J. Electrochem. Soc. 151 (2004) A23.
[28] Y. Sasaki, S. Sekiya, M. Handa, K. Usami, J. Power Sourc. 79 (1999) 91.
[29] Y. Sasaki, M. Handa, K. Kurashima, T. Tonuma, K. Usami, J. Electrochem. Soc. 148 (2001) A999.
[30] N. Nanbu, T. Shibazaki, Y. Sasaki, Electrochemistry 71 (2003) 1205.
[31] N. Nanbu, T. Ebina, H. Uno, Y. Miyazaki, Y. Sasaki, Electrochem. Solid State Lett. 9 (2006) A482.
[32] U. Wietelmann, U. Lischka, K. Schade, J.-C. Panitz, DE 10108608 A1, 2002.
[33] U. Wietelmann, J.-C. Panitz, in: 21st International Seminar & Exhibition on Primary & Secondary Batteries, Fort Lauderdale, USA, 2004.
[34] K. Xu, S.P. Ding, T.R. Jow, J. Electrochem. Soc. 146 (1999) 4172.
[35] J.M. Vollmer, A. Kandalam, P. Zapol, L.A. Curtiss, C. Chen, D.R. Vissers, K. Amine, in: G. Nazri, R. Koetz, B. Scrosati, B.A. Moro, E.S. Takeuchi (Eds.), Advanced Batteries and Super Capacitors, The Electrochemical Society Proceedings Series, PV 2001-20, Pennington, NJ, 2001, p. 389.
[36] Y.-K. Han, J. Jung, J.-J. Cho, H.-J. Kim, Chem. Phys. Lett. 368 (2003) 601.
[37] R.L. Wang, L.M. Moshurchak, W.M. Lamanna, M. Bullinski, J.R. Dahn, J. Electrochem. Soc. 155 (2008) A66.
[38] T. Li, L. Xing, W. Li, B. Peng, M. Xu, F. Gu, S. Hu, J. Phys. Chem. A 115 (2011) 4988.
[39] R.S. Assary, L.A. Curtiss, P.C. Redfern, Z. Zhang, K. Amine, J. Phys. Chem. C 115 (2011) 12216.
[40] P. Johansson, P. Jacobsson, J. Power Sourc. 153 (2006) 336.
[41] J.M. Vollmer, L.A. Curtiss, D.R. Vissers, K. Amine, J. Electrochem. Soc. 151 (2004) A178.
[42] R.L. Wang, C. Buhrmester, J.R. Dahn, J. Electrochem. Soc. 153 (2006) A445.
[43] S. Miertus, E. Scrocco, J. Tomasi, Chem. Phys. 55 (1981) 117.
[44] V. Barone, M. Cossi, J. Phys. Chem. A 102 (1998) 1995.
[45] M. Cossi, N. Rega, G. Scalmani, V. Barone, J. Comput. Chem. 24 (2003) 669.
[46] M.W. Schmidt, K.K. Baldridge, J.A. Boatz, S.T. Elbert, M.S. Gordon, J.H. Jensen, S. Koseki, N. Matsunaga, K.A. Nguyen, S. Su, T.L. Windus, M. Dupuis, J.A. Montgomery, J. Comput. Chem. 14 (1993) 1347.
[47] M.S. Gordon, M.W. Schmidt, in: C.E. Dykstra, G. Frenking, K.S. Kim, G.E. Scuseria (Eds.), Theory and Applications of Computational Chemistry: The First Forty Years, Elsevier, Amsterdam, 2005, p. 1167.
[48] B.M. Bode, M.S. Gordon, J. Mol. Graphics Model. 16 (1998) 133.
[49] A.D. Becke, J. Chem. Phys. 98 (1993) 5648.
[50] A.D. Becke, Phys. Rev. A 38 (1988) 3098.
[51] S.H. Vosko, L. Wilk, M. Nusair, Can. J. Phys. 58 (1980) 1200.
[52] C. Lee, W. Yang, R.G. Parr, Phys. Rev. B 37 (1988) 785.
[53] R.S. Mulliken, J. Chem. Phys. 23 (1955) 1833, 1841, 2338, 2343.
[54] P.O. Löwdin, Adv. Quantum Chem. 5 (1970) 185.
[55] P. Johansson, J. Phys. Chem. A 110 (2006) 12077.
[56] P. Johansson, J. Phys. Chem. A 111 (2007) 1378.
[57] M. Winter, J.O. Besenhard, M.E. Spahr, P. Novák, Adv. Mater. 10 (1998) 725.
[58] G.V. Zhuang, K. Xu, T.R. Jow, P.N. Ross Jr., Electrochem. Solid State Lett. 7 (2004) A224.
[59] K. Xu, U. Lee, S. Zhang, J.L. Allen, T.R. Jow, Electrochem. Solid State Lett. 7 (2004) A273.
[60] K. Xu, U. Lee, S. Zhang, M. Wood, T.R. Jow, Electrochem. Solid State Lett. 6 (2003) A144.
[61] L. Yang, T. Markmaitree, B.L. Lucht, J. Power Sourc. 196 (2011) 2251.
[62] D. Guyomard, in: 5th International Conference on Advanced Lithium Batteries for Automobile Applications (ABAA), Istanbul, 2012.